Journal of Materials Chemistry B

RSC Publishing

PAPER

View Article Online
View Journal | View Issue

Cite this: J. Mater. Chem. B, 2013, 1, 4320

Bifunctional nanoparticles for SERS monitoring and magnetic intervention of assembly and enzyme cutting of DNAs†

Liqin Lin,[ab] Elizabeth Crew,[a] Hong Yan,‡[a] Shiyao Shan,[a] Zakiya Skeete,[a] Derrick Mott,[c] Tatiana Krentsel,[a] Jun Yin,[a] Natasha A. Chernova,[a] Jin Luo,[a] Mark H. Engelhard,[d] Chongmin Wang,[d] Qingbiao Li[b] and Chuan-Jian Zhong*[a]

Received 29th March 2013
Accepted 27th June 2013

DOI: 10.1039/c3tb20446d

www.rsc.org/MaterialsB

The ability to harness the nanoscale structural properties is essential for the exploration of functional properties of nanomaterials. This report demonstrates a novel strategy exploring bifunctional nanoparticles for spectroscopic detection and magnetic intervention of DNA assembly, disassembly, and enzyme cutting processes in a solution phase. In contrast to existing single-function based approaches, this strategy exploits magnetic MnZn ferrite nanoparticles decorated with gold or silver on the surface to retain adequate magnetization while producing sufficient plasmonic resonance features to impart surface-enhanced Raman scattering (SERS) functions. The decoration of MnZn ferrite nanoparticles with Au or Ag (MZF/Au or MZF/Ag) was achieved by thermally activated deposition of Au or Ag atoms/nanoparticles on MZF nanoparticles. Upon interparticle double-stranded DNA linkage of the MZF/Au (or MZF/Ag) nanoparticles with gold nanoparticles labeled with a Raman reporter, the resulting interparticle "hot spots" are shown to enable real time SERS monitoring of the DNA assembly, disassembly, or enzyme cutting processes, where the magnetic component provides an effective means for intervention of the biomolecular processes in the solution. The unique bifunctional combination of the SERS "hot spots" and the magnetic separation capability serves as the first example of bifunctional nanoprobes for biomolecular recognition and intervention.

Introduction

The ability to harness the nanoscale functional properties is essential for the exploration of technological applications of nanomaterials. In medical diagnostics and treatments, two of the functional properties that have been the subjects of broad interest for biomolecular recognition include signal transduction and activity intervention. Signal transduction of biomolecules such as DNAs, proteins, or enzymes has been a focal area of intensive research on various pathogens.[1–3] Many optical and spectroscopic tools are powerful for signal transduction due to their multiplexing or fingerprinting capabilities,[4–19] which often involve immobilization of reporter labels on gold or silver nanoparticles (Au or Ag NPs) on a solid substrate. One example involves targeting of oligonucleotides using nanoparticles functionalized with a specific sequence of oligonucleotides along with a dye label.[4] For most of the existing approaches which involved planar gold or silver substrates as supports for the nanoparticles,[4,6,7,12–14,17] the uncontrollable aggregation of the nanoparticles constitutes a major complication. In contrast, the interparticle plasmonic coupling, a phenomenon originating from the formation of small clusters of NPs such as dimers and trimers,[12] as described in the present report, functions as a spectroscopic nanoprobe to biomolecular processes in solutions where the interparticle chemistry can be well defined by the biomolecules. On the other hand, an effective means is needed for activity intervention of the biomolecular processes in a solution. While the magnetic properties of magnetic nanoparticles (MNPs) have been exploited for bioseparation, controlled delivery, specific targeting, or magnetic resonance imaging (MRI),[20–22] the direct use of many existing metal oxides (*e.g.*, iron or cobalt oxides) in biological fluids is problematic considering their potential toxicity and limited surface chemistry. To impart the desired biocompatibility and surface functionality to MNPs, the surface functionalization of MNPs with gold or silver is one important approach in view of the rich surface chemistry for DNAs, proteins and other

[a]Department of Chemistry, State University of New York at Binghamton, Binghamton, New York 13902, USA. E-mail: cjzhong@binghamton.edu

[b]Environmental Science Research Center, College of Environment and Ecology, Xiamen University, Xiamen 361005, China

[c]School of Materials Science, Japan Advanced Institute of Science and Technology, 1-1 Asahidai, Nomi, 923-1292 Ishikawa, Japan

[d]EMSL, Pacific Northwest National Laboratory, Richland, Washington 99352, USA

† Electronic supplementary information (ESI) available: Additional data for the synthesis and the experimental measurements. See DOI: 10.1039/c3tb20446d

‡ Present address: Institute of Materials Research and Engineering, A*STAR, 3 Research Link, Singapore 117602.

biomolecules.[23] While this approach is supported by our earlier studies on gold-coated MNPs in biomolecular separation from solutions to a solid substrate,[12,13] and other studies such as MNPs on a planar gold substrate,[24] Fe_3O_4@Au NPs labeled with dyes,[25] silver-embedded MNPs for cancer-cell targeting and imaging,[26,27] and SERS detection of DNAs *via* various nanostructures,[28–32] most of them rely either on using solid substrates with immobilized NPs or magnetic enrichment of DNA-particle aggregates separated from the solution state for the detection. There has been no real demonstration of signal transduction and bioactivity intervention through the direct plasmonic coupling of DNA-linked magnetic nanoparticles in the solution and in real time.

We demonstrate herein the first example of a novel bifunctional strategy for signal transduction and activity intervention using Ag- and Au-decorated magnetic MnZn ferrite NPs (MZF/Ag and MZF/Au). In our previous work, MnZn ferrite type NPs were shown to form a core–shell nanostructure consisting of a Fe_3O_4 core and a $MnZnFe_2O_4$ type shell.[33] In comparison with Fe_3O_4 NPs,[34,35] the magnetic properties of such magnetic nanoparticles are tunable by Mn/Zn doping in the shell. In the present work, the Mn/Zn-doped magnetic nanoparticles were decorated with Au or Ag by a thermally activated processing technique,[13,14] which allows controllable deposition of the metals on the magnetic NPs under thermal heating conditions.[13] The choice of the Au or Ag decoration, rather than a full shell, stems largely from the consideration of retaining the magnetization. Magnetic NPs fully coated by Au were shown to reduce the magnetization significantly.[34] In this report, we demonstrate that the Au or Ag decoration on the magnetic NPs not only allows effective exploitation of the magnetic properties, but also allows effective exploration of the plasmonic properties for surface-enhanced Raman scattering (SERS). A key element to enable an effective magnetic function is that the Au or Ag layer on the magnetic particles should not be too thick to significantly reduce the magnetization,[34] while they are sufficient to produce the plasmonic resonance coupling for SERS. These features would allow SERS detection and magnetic intervention of DNA assembly, disassembly, and enzyme cutting processes in aqueous solutions. In contrast to the previous studies,[28–32] there are several important attributes in our strategy. The use of Au- or Ag-decorated magnetic nanoparticles introduces magnetic

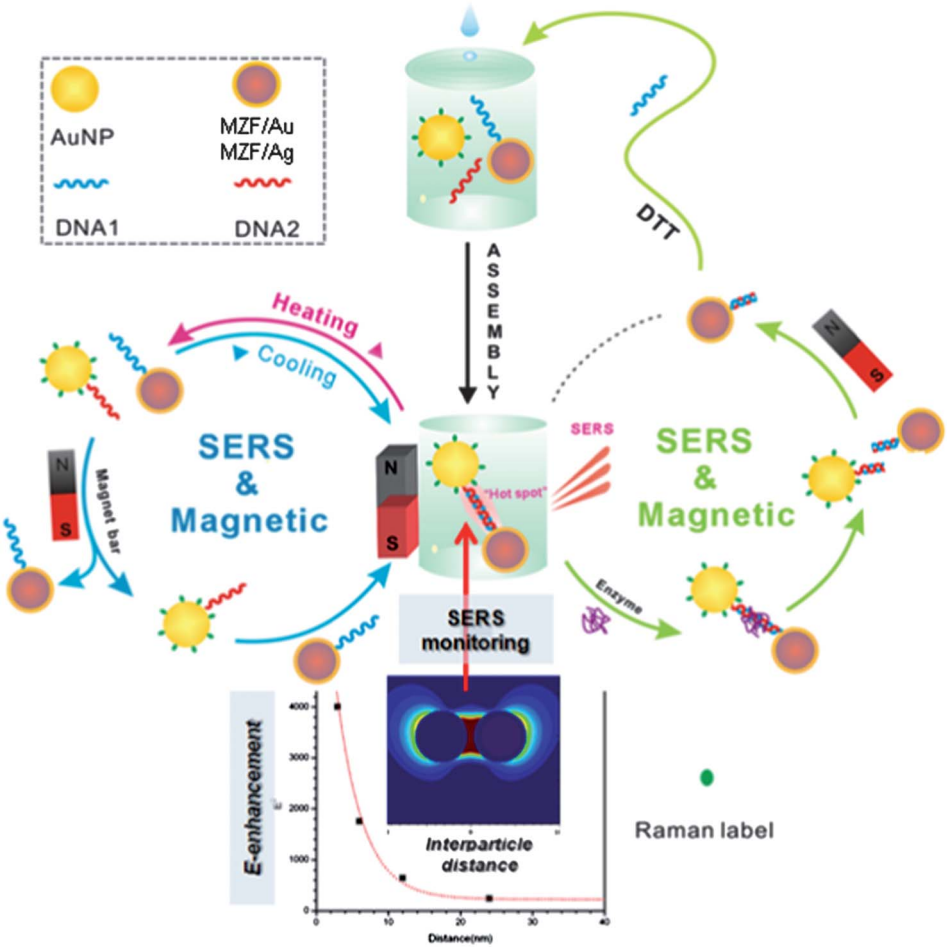

Scheme 1 An illustration of the bifunctional strategy exploiting the multifunctional NPs for SERS detection and magnetic intervention of DNA assembly, disassembly, and enzyme cutting processes in the solution. These processes involve interparticle "hot-spot" formation and magnetic removal. Bottom panel: correlation between the theoretically calculated enhanced electric field and the spacing of Ag nanoparticle dimers. Inset: a contour external to a dimer of Ag nanoparticles (60 nm) with a certain spacing (see Fig. S1† for details).

functionality in the direct recognition of two DNA strands anchored respectively to two different nanoparticles, *i.e.*, Raman-labeled Au NPs ("Raman probe") and Au- or Ag-decorated magnetic NPs ("Magnetic (Mag) probe"), which are illustrated in Scheme 1 for the biomolecular processes involving assembly and disassembly of two complementary ss-DNAs (DNA1 and DNA2), and the enzyme cutting of the ds-DNA. One ss-DNA is attached to Au NPs labeled with a Raman label molecule (Au NPs-R) and the other being anchored to the magnetic MZF/Au or MZF/Ag NPs. The interparticle plasmonic coupling as a result of the ds-DNA linkage creates a "hot-spot" which provides a means for SERS detection of the assembly and the disassembly either by restriction enzyme cleavage of the ds-DNA or by thermal removal of the hydrogen-bonding between the base pairs. The magnetic component of the nanoprobes provides the capabilities of magnetic intervention, bioseparation, resuspendability, and potential recyclable or sustainable uses.

The foundation for the SERS function stems from theoretical calculation of the local electric field enhancement (*i.e.*, "hot-spot") for a dimer of NPs using the discrete dipole approximation method,[36] which reveals an E-field enhancement that is dependent on the interparticle spacing in the dimer (see ESI, Fig. S1†). The E-field enhancement increases sharply with the reduction of the interparticle spacing. When the interparticle spacing increases, the E-field enhancement weakens. For a dimer of DNA1–MNP and MBA-Au NPs by DNA2 *via* binding of the complementary base pairs as described in this report, the interparticle spacing under an ideal interparticle ds-DNA linking is estimated to be about 10 nm in length, which falls into the "hot spot" region (ESI, Fig. S1†). When an enzyme cuts the ds-DNA at a specific site, or the solution is heated to induce a disassembly of the dimer, the interparticle spacing increases and eventually the two NPs are separated, leading to weakening and disappearance of the "hot spot". This type of "hot spot" formation/removal, coupled with the magnetic functionality, constitutes the basis of the SERS detection and activity intervention in the DNA assembly and disassembly processes. In comparison with the SERS-only detection using pure Au NPs,[37] this "Raman-Magnetic" probe could enable interparticle "hot spot" formation and bio-separation capability for monitoring DNA assembly and cutting processes in the solution phase and in real time, which is to our knowledge the first example of this kind of bifunctionality.

Experimental

Chemicals and nanoparticles

Hydrogen tetrachloroaurate(III) hydrate ($HAuCl_4 \cdot xH_2O$), silver nitrate ($AgNO_3$), sodium hydroxide, sodium acrylate (97%), sodium chloride (NaCl, 99%), ethylenediaminetetraacetic acid (EDTA), 4-mercaptobenzoic acid (MBA), oleylamine (OAM, 70%), benzyl ether, 1-decanethiol (DT, 99%), and 11-mercaptoundecanoic acid (MUA, 97%) were purchased from Sigma-Aldrich (Milwaukee, WI) and used as received. Iron(III) acetylacetonate ($Fe(acac)_3$, 99%, Lancaster), manganese(II) acetylacetonate ($Mn(acac)_2$, 95% Strem), zinc acetylacetonate ($Zn(acac)_2$, 98%, Strem), and oleic acid (OAC, 99%, Alfa Aesar) were also used for the synthesis. Phosphate buffer was purchased from Fisher Scientific (Pittsburgh, PA). Thiol modified DNAs with standard desalting purification were purchased from Integrated DNA Technologies, Inc. (Coralville, IA). NAP-5 columns were purchased from GE Healthcare (Uppsala, Sweden) and *MspI* from New England Biolabs (Beverly, MA). The solvents including hexane (99.9%) and toluene (99.8%) were from Fisher. Water was purified with a Millipore Milli-Q water system.

Nanoparticle synthesis

Au NPs and Ag NPs of 2 nm in size encapsulated with DT monolayer capping molecules were synthesized based on the standard and modified two-phase method.[13,38,52]

The synthesis of MZF nanoparticles was based on a method developed in our laboratory,[33,39] which involved thermal decomposition of metal acetylacetonate compounds, *e.g.*, 0.469 g $Fe(acac)_3$, 0.081 g $Mn(acac)_2$, and 0.087 g $Zn(acac)_2$ in 20 mL of benzyl ether with 2 mL of oleic acid and 2 mL of oleylamine. The mixture was refluxed for 60 min. The product was collected using a magnet.

For the preparation of MZF/Au and MZF/Ag nanoparticles, a modified strategy of the thermally activated processing protocol was used.[13] In a typical synthesis, 1.3 mL of concentrated Au-DT (or Ag-DT) and MZF nanoparticles (*e.g.*, stock solutions of DT-capped Au (2 nm, 33 μM) and OAM/OAC-capped MZF (8 nm, 2.6 μM)) in toluene with a certain ratio was placed in a reaction tube. The tube was then placed in a preheated Yamato DX400 gravity convection oven at 150 °C for 3 h. Temperature variation from this set point was limited to 1.5 °C. After the thermal treatment, the reaction tube was allowed to cool down, and the particles were re-dispersed in toluene.

DNA assembly/disassembly procedures

The as-synthesized DT-capped MZF/Au and MZF/Ag particles were transferred to water by ligand exchange using mercaptoundecanoic acid (MUA) by following a procedure reported by Gittins and Caruso with a slight modification.[53] Then the NPs were further modified with DNA for assembly and SERS detection. The detailed procedures for the assembly and the restriction enzymes cutting areas were reported previously,[12,46] and are summarized below.

MZF/Au (or MZF/Ag) and Au NP assembly based on complementary oligonucleotides

To demonstrate the viability of assembly between MZF/Au (or MZF/Ag) and Au NPs, two different DNAs (DNA1: 5′-/5ThioMC6-D/AGGCCAGACCTGCCCGGGCAAGCCTTGGCA-3′ (bottom strand) and DNA2: 5′-/5ThioMC6-D/TGCCAAGGCTTGCCCGGGCAGGT CTGGCCT-3′ (top strand)) were used. Acrylate-capped Au NPs with an average size of 39.7 ± 1.8 nm were synthesized following the procedure reported previously.[8] DNA1 and DNA2 were first dissolved in 0.1 M phosphate buffer (pH 8) at a concentration ranging from 300 to 370 μM. The disulfide bonds in DNA1 and DNA2 were cleaved using an approach similar to the reported

procedure,[46] where dithiothreitol (DTT) at a final concentration of 0.1 M was added to ~10 OD of the nucleotides in a final volume of 400 μL. The solution was allowed to react at room temperature for 2 h, then poured through a NAP-5 column and an aliquot of 1.1 mL phosphate buffer (pH 8) was added to the column to elute the cleaved oligonucleotide. The final concentration of the cleaved DNAs was 10 μM with an OD 260 nm of 3.6. The exact concentrations of DNAs varied slightly depending on the specific experiment.

The surface of MZF/Au (or MZF/Ag) was functionalized with the cleaved DNA1 similar to the reported procedure[46] to form MZF/Au–DNA1 (or MZF/Ag–DNA1). Briefly, 0.176 mL of the cleaved DNA1 was added to 3 mL of MZF/Au nanoparticles (or MZF/Ag nanoparticles). The solution was left standing at room temperature for 16 h, after which it was diluted to 20 mM NaCl and 10 mM phosphate buffer (pH 7) and allowed to stand for another 40 h at room temperature. The DNA1-capped nanoparticles were then centrifuged and washed twice at 14 000 rpm (18 620*g*) for 25 min (each time the solution was re-dispersed in a 20 mM NaCl/10 mM phosphate buffer (pH 7) solution) before being re-dispersed in its final (20 mM NaCl/10 mM phosphate buffer/0.01% sodium azide (pH 7)) solution and stored at room temperature.

The MBA-Au NPs: a controlled volume of 0.1 mM MBA for a 50% surface coverage was added to 3 mL of Au NPs (stock concentration 0.1 nM). The solution was left standing at room temperature overnight before use. The estimate of this coverage was based on the measurement of an adsorption isotherm, *i.e.*, the SERS intensity *vs.* concentration of MBA.[12]

To study the assembly of the DNA capped MZF/Au (or MZF/Ag) nanoparticles with 39 nm Au NPs, 17 μL of DNA2 was added to 300 μL of MZF/Au–DNA1 (or MZF/Ag–DNA1) in the presence of 300 μL of MBA-labeled Au NPs. The reaction was monitored by UV-Vis and Raman spectroscopy.

Restriction enzyme cutting

For the enzyme cutting experiment, the restriction enzyme *MspI* (100 units per μL) was utilized. 5 μL of restriction enzyme was added to 350 μL of the assembled solution, along with the buffer for the restriction enzyme. The solution was incubated at 37 °C (*MspI*) with constant stirring and the Raman spectrum was taken at different time intervals.

Instrumentation and measurements

UV-Visible (UV-Vis) spectra were acquired with a Hewlett Packard 8453 spectrophotometer.

Transmission electron microscopy (TEM) was performed on a Hitachi H-7000 Electron Microscope (100 kV). The TEM samples were prepared by taking a solution sample and casting it onto a carbon-coated copper grid sample holder followed by evaporation in air at room temperature. HRTEM analysis was carried out using a JEOL JEM 2010F at an acceleration voltage of 200 kV. The nanoparticles were diluted in hexane solvent and drop cast onto a carbon-coated copper grid, followed by solvent evaporation in air at room temperature. HRTEM in PNNL analysis was carried out on a JEOL JEM 2010F microscope with a specified point-to-point resolution of 0.194 nm. The operating voltage of the microscope was 200 kV. High-angle annular dark-field scanning TEM (HAADFSTEM) imaging for morphology characterization and energy dispersive X-ray spectroscopy (EDS) for elemental mapping were carried out on an JEOL JEM-ARM200F instrument operated at 200 kV with a spherical aberration corrector.

Surface-enhanced Raman scattering (SERS) spectra were recorded using an Advantage 200A Raman spectrometer (DeltaNu) and the data were collected from 200 to 2000 cm^{-1}. The laser power and wavelength were 5 mW and 632.8 nm, respectively. The scattering geometry utilized was backscattering.

Inductively coupled plasma-optical emission spectroscopy (ICP-OES) was used to analyze the nanoparticle composition. It was performed on a Perkin-Elmer 2000 DV ICP-OES with the following parameters: plasma, 18.0 L of Ar(g) min^{-1}; auxiliary, 0.3 L of Ar(g) min^{-1}; nebulizer, 0.73 L of Ar(g) min^{-1}; power, 1500 W; and peristaltic pump rate, 1.40 mL min^{-1}. Reported values of <1.0 mg L^{-1} were analyzed using a Meinhard nebulizer coupled to a cyclonic spray chamber to increase the analyte sensitivity. Elemental concentrations were determined by measuring one or more emission lines (in nm) to check for interferences.

X-ray Photoelectron Spectroscopy (XPS) measurements were performed on a Physical Electronics 5000 versa probe scanning ESCA microprobe. The system uses a focused monochromatic Al Kα X-ray (1486.7 eV) source for excitation and a spherical section analyzer. The instrument has a 16-element multichannel detection system. Wide scan data were collected using a pass energy of 187.85 eV. The binding energy (BE) scale was calibrated using Cu 2p3/2 line at 932.58 ± 0.05 eV and Au 4f7/2 line at 84.01 ± 0.05 eV. The sample experienced variable degrees of charging by low energy electrons at ~1.5 eV, 20 μA so that low energy Ar^+ ions needed to be used to minimize this charging. The percentages of individual elements detected were determined from the relative composition analysis of the areas of the XPS lines.

Superconducting quantum interference device (SQUID): The dc magnetization and magnetic susceptibility were measured using a magnetometer Quantum Design MPMS XL-5. Before the measurements, a possible remnant magnetic field was removed using the ultralow-field option at 298 K. The resultant remnant field was less than 3 mOe. The measurements of the dc magnetization and magnetic susceptibility were carried out after appropriate cooling procedures. The details of the cooling protocol for each measurement are described in the Discussion.

Results and discussion

Characterization of MZF/Au and MZF/Ag NPs

The as-synthesized MZF NPs feature about 8 nm in size and roughly cubical shape as reported recently.[33] MZF NPs of several slightly different ratios were utilized for the decoration by Au or Ag. For example, an MZF with an Fe : Mn : Zn ratio of 84 : 8 : 8 consisted of a Fe_3O_4 core and a $(Mn_{0.5}Zn_{0.5})Fe_2O_4$ shell with a shell to core volume ratio of 1 : 1.1 on the basis of our previous study.[33] The shell was about 48% (vol) (*i.e.*, % of the volume of

the shell relative to the whole core–shell volume), which is ~0.8 nm in shell thickness for the 8 nm MZF NP. The MZF/Au and MZF/Ag NPs, prepared by the thermally activated processing of the MZF NPs and Au (2 nm) or Ag NPs (2 nm) at or near their nanoscale melting temperatures,[13,14,38] featured 11 and 9 nm in sizes. Based on the elemental composition from ICP data, the shell thickness was estimated to be ~0.3 nm for Au and ~0.1 nm for Ag, which appeared to be quite consistent with the EDS composition mapping data (as described later). This set of MZF/Au and MZF/Ag NPs was mainly used for the demonstration of the bifunctional properties for assembly, disassembly and enzyme cutting of DNAs.

In another set of MZF/Au and MZF/Ag NPs, MZF of a similar composition was used for the decoration by Au or Ag, which corresponds to the Fe_3O_4 core and the $(Mn_{0.5}Zn_{0.5})Fe_2O_4$ shell with a shell to core ratio of 1 : 3.2. This shell is about 24 vol%, which is 0.4 nm in shell thickness for the 8 nm MZF NP. The MZF/Au and MZF/Ag NPs, prepared by the same thermally activated processing,[13,14,38] also featured 11 and 9 nm in sizes. Based on the elemental composition from ICP data, the shell thickness was estimated to be ~1.0 nm for Au and ~1.4 nm for Ag, which appeared much larger than those found by the EDS mapping analysis. Due to the presence of pure Au or Ag nanoparticles in the Au or Ag decorated MZF samples, the actual thickness is believed to be much smaller, as supported by HRTEM and EDS mapping data. This set of MZF/Au and MZF/Ag NPs was mainly used for the determination of the magnetic properties as discussed next.

The functional properties of the MZF/Au and MZF/Ag NPs were first assessed by monitoring the changes in the surface plasmon resonance bands from the Au or Ag component and the magnetic function from the MZF component for a solution of the nanoparticles in a cell (see ESI, Fig. S2 and S3†). The experiment data revealed clearly a gradual decrease of the surface plasmon resonance bands upon applying a magnetic bar to the solution cell (Fig. S2 and S3†), similar to those reported recently.[13,39] The fact that the experimental plasmonic resonance absorption spectra spanned to the near IR region is consistent with the theoretical simulation results that the surface plasmonic (SP) resonance band shifts from the visible to near infrared region as shell thickness decreases (see ESI, Fig. S4†), suggesting that the MZF/Au or MZF/Ag nanoparticles likely have various shell thicknesses.

More importantly, XPS analysis of the relative changes in the metal composition and binding energies for samples of MZF, MZF/Au and MZF/Ag NPs also revealed intriguing interactions between Au (or Ag) shell and MZF core (see Fig. S5 and Table S1†). The positive shift of binding energy (BE) for Au 4f in comparison with gold and the negative shift for Fe 2p and Zn 2p in comparison with MZF (Table S1†) indicated a charge transfer from gold to iron/zinc for MZF/Au. This suggests the presence of Au atoms in the surface lattice of the spinel MZF, which is in agreement with previous studies.[40,41] For MZF/Ag, while a similar positive shift of BE for Fe 2p and Zn 2p (Table S1†) was observed, suggesting a similar charge transfer to iron/zinc, the BE for Ag 3d showed a negative shift in comparison with silver, reflecting the dominance of a strongly bound oxygen at the silver surface.[42] The latter suggests the presence of Ag–O–Fe/Zn type of interaction for the silver layer on the surface lattice of the spinel structure.

HRTEM images of nanoparticles before and after coating Au or Ag were carefully analyzed in terms of the atomic lattices (Fig. 1), similar to those reported previously.[43–45] For MZF, the measured lattice fringe (0.302 nm) corresponds to the (220) plane of the spinel structure (Fig. 1A). For MZF/Au, the MZF's lattice fringe (0.302 nm) is still evident, but the lattice fringe (0.240 nm) corresponding to the (111) plane of Au is also observed (Fig. 1B). For MZF/Ag, nanoparticles with different morphologies such as dumbbell-like structure were also observed, as supported by the observation of the lattice fringe (0.240 nm) that corresponds to (110) of Ag and the lattice fringe (0.291 nm) that can be assigned to (220) of MZF nanoparticles (Fig. 1C). It is believed that the surface coverage of MZF NPs by Au or Ag is likely incomplete.

As shown by the EDS data for MZF/Au and MZF/Ag nanoparticles (Fig. 2), distributions of the expected components, Fe, Mn, Zn, and Au or Ag, can be identified. The predominance of Fe is consistent with the composition data for MZF (Fe : Mn : Zn = 84 : 8 : 8). The relative distribution of Au or Ag in terms of quantity seems to be somewhat less than or similar to that of Mn or Zn in MZF. By overlapping Fe and Au in the case of MZF/Au or Fe and Ag in the case of MZF/Ag, there is clear indication showing that Au or Ag metals are decorated on the MZF. This observed decoration of Au or Ag on the MZF is consistent with the absence of lattices of Au or Ag on the MZF as observed in the HRTEM data (Fig. 1).

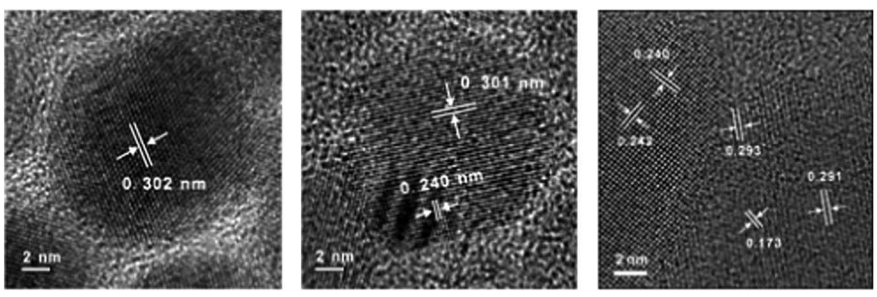

Fig. 1 HRTEM images for samples from (A) MZF, (B) MZF/Au and (C) MZF/Ag nanoparticles.

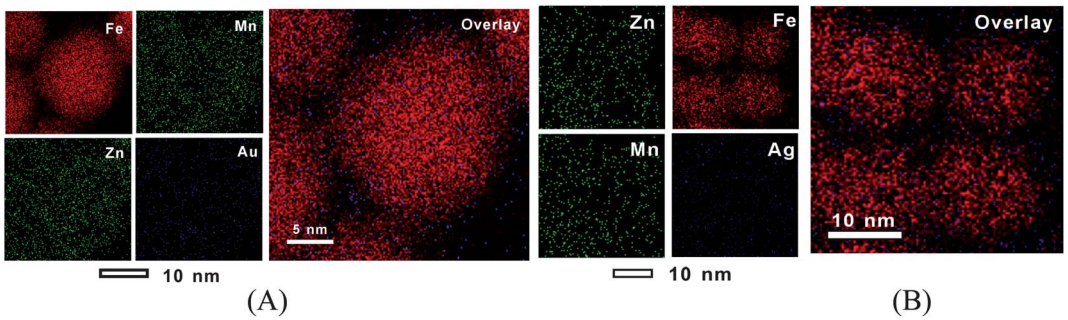

Fig. 2 EDS composition mapping for samples of (A) MZF/Au and (B) MZF/Ag nanoparticles in terms of individual components Fe, Mn, Zn and Au or Ag, and their overlapping of Fe and Au (for MZF/Au) and Fe and Ag (for MZF/Ag).

The MZF/Au and MZF/Ag were examined in terms of saturation magnetization, coercivity, and blocking temperature based on SQUID measurements. In this case, the sample with a shell thickness of ~1.0 nm for Au or ~1.4 nm for Ag was used. The saturation magnetization was measured at 2 K with an applied field of −50 to 50 kOe. Fig. 3 shows a representative set of data for MZF/Au (similar data were also obtained for MZF/Ag). As shown in Fig. 3A, the highest value of magnetization was found to be 93 emu g^{-1} (for MZF/Ag ~ 55 emu g^{-1}). Note that the maximum magnetization values for Fe_3O_4 (5.2 nm) and core–shell MZF of a slightly different composition (~20 nm) were previously reported to be 66 emu g^{-1},[34,35] and 46 emu g^{-1},[33] respectively. While the differences can be attributed to a combination of differences in particle size, composition, and Mn/Zn doping sites, the fact that there is such a high value of magnetization suggests a very thin coating of Au on the surface of MZF.

The coercivity value was about 288 Oe for MZF/Au at 2 K (for MZF/Ag ~312 Oe). This value is much higher than that for the Fe_3O_4 nanoparticles (40 Oe) at 5 K,[34] and slightly smaller than the core–shell nanocubes (Fe_3O_4 core@$(Mn_{0.5}Zn_{0.5})(Fe_{0.9}Mn_{1.1})O_4$ shell).[33]

The zero-field-cooled (ZFC) and field-cooled (FC) curves for MZF/Au are shown in Fig. 3B. Interestingly, the ZFC/FC characteristic does not resemble that observed for the core–shell nanocube (Fe_3O_4 core@$(Mn_{0.5}Zn_{0.5})(Fe_{0.9}Mn_{1.1})O_4$ shell).[33] Rather, it is quite similar to that for Fe_3O_4 NPs.[34] This feature is believed to likely reflect the presence of a very thin MZF shell around the Fe_3O_4 nanoparticles, in contrast to the core–shell nanocubes with a thick $MnZnFe_2O_4$ shell around the Fe_3O_4 core.[33] The blocking temperature (T_b) is determined to be 61 K for MZF/Au (for MZF/Ag ~70 K), which is higher than that for pure Fe_3O_4 nanoparticles (17 K). The fact that the sample has a much higher T_b than those for pure Fe_3O_4 (17 K) and Fe_3O_4 (5 nm core)@Au (1 nm shell) (13 K) is also consistent with the composition analysis data discussed earlier.

ss-DNA assembly and ds-DNA disassembly

To demonstrate the bifunctionality of the nanoprobes, two complementary 30-bp DNA sequence oligonucleotide strands with a thiol group at one end, 5′-/5ThioMC6-D/AGGCCA GACCTGCCCGGGCAAGCCTTGGCA-3′ (DNA1) and 5′-/5ThioMC6-D/TGCCAAGGCTTGCCCGGGCAGGTCTGGCCT-3′ (DNA2), were used. The conjugation of MZF/Au (or MZF/Ag) with the DNA1 was similar to the reported procedure[46] to form MZF/Au–DNA1, and the labeling of Au NPs with mercaptobenzoic acid (MBA-Au) was achieved by following a previously reported procedure.[12] For the disassembly process, the restriction enzyme *MspI* (100 units per μL) was utilized and the procedure was similar to our previous report[46] (see ESI† for more details). Note that the use of TEM by casting solution samples to visualize dimers or trimers may not be appropriate because it could lead to various ensembles depending on particle concentration, evaporation rate, and other factors. Technically, it was very difficult to avoid random aggregation,

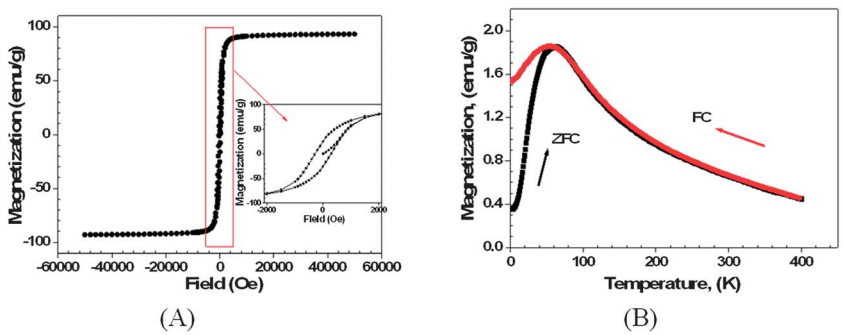

Fig. 3 Magnetization curves for the MZF/Au sample. SQUID measurements of magnetization hysteresis curves (A) (Inset: magnification of the curves near zero Oe), and field-cooled (FC) and zero-field-cooled (ZFC) curves (B).

and a further study using different grid preparation techniques may provide additional information, which will be our future work. The following two sections focus on their novel SERS and magnetic characteristics for the demonstration of the operation of interparticle "hot spots" in monitoring the DNA assembly, disassembly and enzyme cutting processes.

The assembly of MZF/Au–DNA1 (or MZF/Ag–DNA1) with MBA-Au NPs in the presence of free DNA2 involves complementary oligonucleotide binding of DNA2 strand to the DNA1 strand attached to MZF/Au (or MZF/Ag) NPs (Scheme 2), leading to the formation of small aggregates (dimers, trimers, *etc.*) linked by ds-DNA (MBA-Au–DNA1/DNA2–MZF/Au or MBA-Au–DNA1/DNA2–MZF/Ag) and the creation of "hot spots" for SERS detection. The hydrogen bonds between base pairs in the ds-DNA deactivate when the temperature is higher than melting temperature (T_m), leading to a return in the two single strands. This process is reversible. When the temperature is ~30 °C below T_m, the base pairing re-establishes the interparticle "hot spot". However, if a magnetic field is applied to the solution at $>T_m$, which separates the magnetic component, the "hot spots" will not be reestablished upon lowering temperature. Two examples are shown below to demonstrate these processes.

The first example involves the assembly of MZF/Au NPs (11 nm) and MBA-Au NPs (39 nm) by the formation of interparticle ds-DNA of DNA1 and DNA2. Note that the concentration of top-DNA added to the assembly process in this experiment was 0.2 to 2 μM, which was similar to those reported for loading different DNAs on Au NPs, including 2–3 μM,[47] 10 μM,[48] and 3 μM,[4] though much lower concentrations were reported for different systems such as those with 1 pM to 10 fM,[49] and those with nM level detection by separation free SERS assay when target DNA is present using a specifically designed SERS primer.[50] In contrast to the absence of bands in the Raman spectrum for the individual components such as MZF/Au–DNA1 and MBA-Au or their simple physical mixture (Fig. 4A, curves a–c), the addition of DNA2 to the mixed solution leads to the observation of two clear SERS peaks at 1078 and 1592 cm^{-1} (Fig. 4A, curve d), corresponding to the ν(CC) ring-breathing modes of MBA. This finding is indicative of the interparticle "hot-spot" formation due to assembly of MBA-Au–DNA1/DNA2–MZF/Au, forming dimers or trimers in the solution.

When the temperature of the assembly solution was increased to 95 °C, the SERS intensity was found to decrease (Fig. 4B, curves a and b), though the kinetics of decrease was

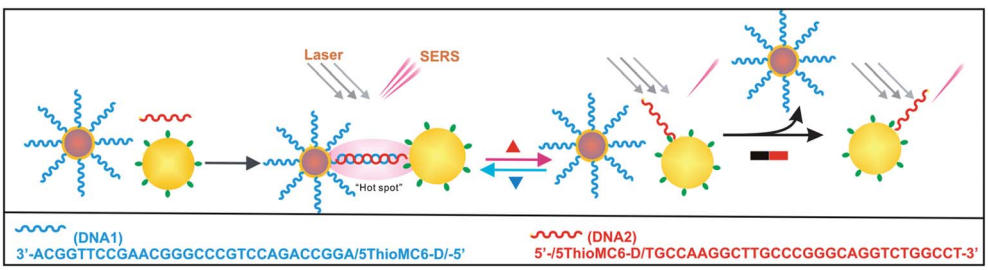

Scheme 2 A schematic diagram illustrating the assembly of MZF/Au–DNA1 (or MZF/Ag–DNA1) with MBA-Au NPs in the presence of DNA2, and the thermal and magnetic intervention of MBA-Au–DNA1/DNA2–MZF/Au (or MZF/Ag) assemblies *via* heating and magnetic separation. DNA1 and DNA2 are complementary 30 bp DNA sequence strands.

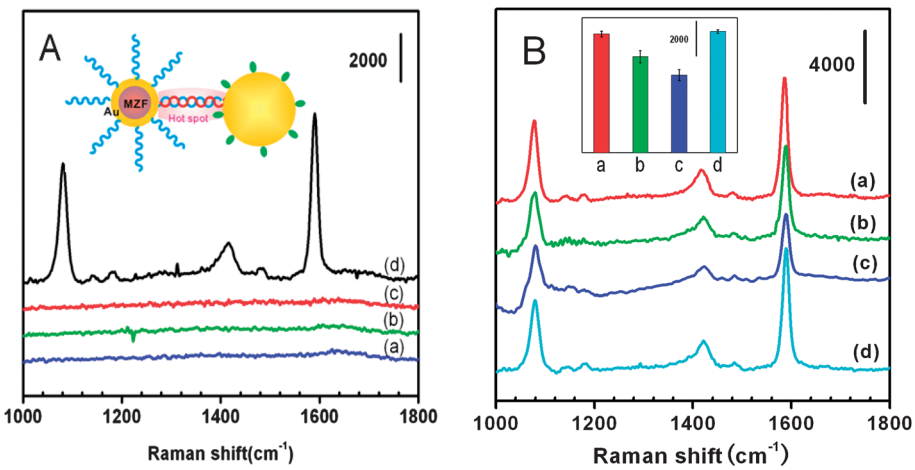

Fig. 4 SERS spectra showing the assembly of MBA-Au NPs and MZF/Au–DNA1 NPs by DNA2 in aqueous solution (A) ((a) MBA-Au (4.3×10^{-2} nM), (b) MZF/Au–DNA1 (6.2 nM), (c) the mixture of MBA-Au and MZF/Au–DNA1, and (d) the mixture of MZF/Au–DNA1 and MBA-Au in the presence of DNA2 (0.56 μM)); and the temperature-induced disassembly of MBA-Au–DNA1/DNA2–MZF/Au (B) ((a) initial sample at 25 °C, (b) 95 °C for 10 min, (c) 95 °C for 10 min followed by applying a magnetic bar to the sample cell for 1 h, and (d) upon releasing MNPs back to the solution at 25 °C; inset: comparison of SERS intensities at 1592 cm^{-1}).

relatively slow. The kinetics could be accelerated by applying a magnetic field to the solution (Fig. 4B, curve c), which removed part of the disassembled MNPs from the solution. By re-dispersing them back into the solution, the intensity was shown to be restored to almost the previous level (Fig. 4B, curve d). This finding demonstrates the viability of a temperature-controlled reversible assembly–disassembly process which can be intervened by a magnetic field.

The second example involves a combination of MZF/Ag NPs (9 nm) and MBA-Au NPs (39 nm) (Fig. 5A). The addition of DNA2 to this mixture solution showed two very strong diagnostic peaks of MBA at 1078 and 1592 cm^{-1} (Fig. 5A, curve d), again in sharp contrast to the very small peaks at 1078 and 1592 cm^{-1} in the solution before adding DNA2 (Fig. 5A, curves a–c). This finding is indicative of the assembly of the two nanoparticle components, forming a dimer or trimer of MBA-Au–DNA1/DNA2–MZF/Ag. The nanoparticle assemblies could also be effectively separated from the solution by applying a magnetic bar, and re-dispersed in a different aqueous solution.

The change in SERS intensity of an MZF/Ag containing system when the temperature of the assembly solution was increased to 95 °C was found to be similar to that in the previous example using MZF/Au as the MNP component, but with an enhanced effectiveness (Fig. 5B). The intensity of two SERS peaks decreased significantly upon increasing the temperature (Fig. 5B, curve b), indicating an effective disassembly. When the MNPs were removed by applying a magnetic bar, the SERS remained low (Fig. 5B, curve c). However, the SERS feature was completely restored by redispersing the MZF/Ag NPs back into the solution (Fig. 5B, curve d), similar to the previous case using MZF/Au NPs as the magnetic component (Fig. 4B, curve d).

The magnetic functionality can be clearly visualized of the colorimetric change of the solution by applying a magnetic bar to the side of the sample cell to attract the components associated with the magnetic nanoparticles. Indeed, the DNA-linked small aggregates could be separated from the solution by the magnetic bar and re-dispersed in a fresh solution. This feature is shown by the example in Fig. 6 for both MZF/Au (A) and MZF/Ag (B). The Raman bands in the SERS spectra showed almost the same spectral features and intensities as those before the magnetic separation, demonstrating that the SERS signal originates from the DNA-linked nanoparticle assemblies there were associated with magnetic nanoparticles.

These results clearly revealed a significant SERS effect on the ds-DNA-linked nanoparticle assemblies in the solution. The enhancement factor for the nanoparticle assemblies was estimated for several combinations of the nanoparticles (see Table S2†), yielding 7.1×10^4 for the ds-DNA assembly of MZF/Au and Au NPs, and 1.5×10^5 for the ds-DNA assembly of MZF/Ag and Au NPs. In comparison, experiments using pure Au NPs and Ag NPs to substitute MZF/Au and MZF/Ag, respectively were found to yield EF values of 2.9×10^5 for the assembly of 13 nm Au NPs and 39 nm Au NPs, and 2.8×10^5 for the assembly of 4 nm Ag NPs with 39 nm Au NPs, demonstrating some general agreement with the data for samples containing the MNPs. These EFs were at least one order of magnitude higher than those for unlinked gold nanoparticles in aqueous solution (10^2 to 10^3) which were obtained experimentally and theoretically under the condition of no aggregation,[51] substantiating the important role of the interparticle "hot spots" in SERS. It is important to emphasize that there is no evidence in our experiment or in the literature indicating the SERS effect of the pure magnetic nanoparticles, which is consistent with the lack of effective plasmonic coupling for the pure magnetic particles. As evidenced by the UV-Vis data, the plasmonic band of the pure Au NP is larger than that of the gold-coated magnetic nanoparticles. Thus, the plasmonic coupling of the pure Au NPs is apparently greater than that of the gold-decorated magnetic nanoparticles, leading to an increased enhancement. We did not study the particle size effect at this point, which will be part of our future study.

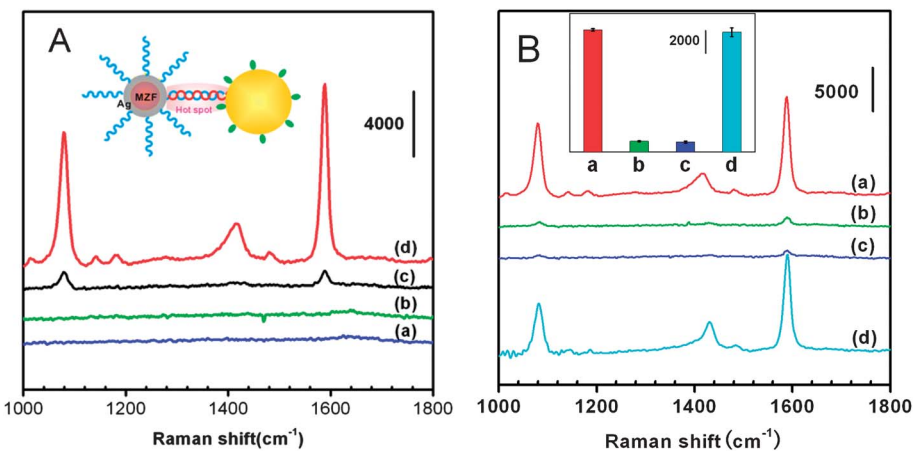

Fig. 5 SERS spectra showing the assembly of MBA-Au NPs and MZF/Ag–DNA1 NPs by DNA2 in aqueous solution (A) ((a) MBA-Au (4.3×10^{-2} nM), (b) MZF/Ag–DNA1 (3.0 nM), (c) the mixture of MBA-Au and MZF/Ag–DNA1, and (d) the mixture of MZF/Ag–DNA1 and MBA-Au in the presence of DNA2 (0.56 μM)); and the temperature-induced disassembly of MBA-Au–DNA1/DNA2–MZF/Ag (B) ((a) initial sample at 25 °C; (b) 95 °C for 10 min, and (c) 95 °C for 10 min followed by applying a magnet to the sample cell for 1 h, and (d) upon releasing magnetic components back to the solution at room temperature).

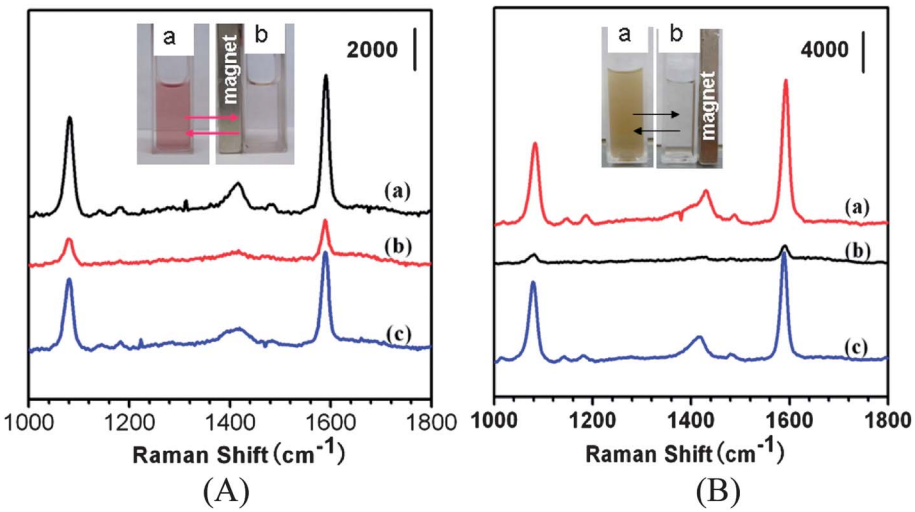

Fig. 6 SERS spectra for assemblies which were separated using a magnetic bar and then re-dispersed in the aqueous solution. (A) ((a) the MBA-Au–DNA1/DNA2–MZF/Au assembly before applying a magnetic bar; (b) the residual assembly solution after magnetic separation; (c) MBA-Au–DNA1/DNA2–MZF/Au assembly separated by a magnetic bar and then re-dispersed in the aqueous solution). (B) ((a) the MBA-Au–DNA1/DNA2–MZF/Ag assembly before applying a magnetic bar; (b) the residual assembly solution after magnetic separation; (c) MBA-Au–DNA1/DNA2–MZF/Ag assembly separated by a magnetic bar and then re-dispersed in the aqueous solution.) Insets: photos showing the corresponding solutions of the nanoparticles before (a) and after (b) applying a magnet.

Enzyme cutting of ds-DNA assembly

For the restriction enzyme (*e.g.*, *MspI*) cleavage of the ds-DNA in the interparticle assembly, the enzymatic cutting leads to the separation of the linked particles into individual particles and removal of the interparticle "hot spots" responsible for the SERS effect (Scheme S1†). In addition to the SERS monitoring, an important feature is the ability to separate the Au NPs and the MNPs after the enzymatic cutting, which can further be recycled after releasing the ds-DNA fragment and ss-DNA from the NPs. The disassembly of the ds-DNA-assembled Au NPs in a solution using restriction enzyme *MspI* and release of the fragment DNAs were demonstrated in elution bands observed in the gel electrophoresis data (inset in Scheme S1†).[46] Two examples are shown below to demonstrate the SERS monitoring of the enzyme cutting and the magnetic intervention processes.

Starting from the solution containing MBA-Au–DNA1/DNA2–MZF/Au assemblies (as shown in Fig. 4), the addition of *MspI* to this solution was shown to display a clear reduction of the two diagnostic peaks of the Raman label MBA-Au–DNA1 (Fig. 7A). The reduction of the peak intensity was relatively fast, reaching ~100% within 1 hour (see Fig. 7A inset). The intensities of the residual peaks were similar to those before the assembly. Note that the MZF/Au NPs after the enzymatic cutting could be separated from the solution by applying a magnetic bar to the sample cell and the DNA fragments could be released chemically, as evidenced by UV-Vis data (Fig. S6†). This example served as a demonstration of recyclability of the bifunctional nanoparticles.

With a solution containing MBA-Au–DNA1/DNA2–MZF/Ag, the addition of *MspI* revealed again a clear reduction of the two SERS peaks as a function of time (Fig. 7B). In comparison with the change observed for the enzymatic cutting of MBA-Au–DNA1/DNA2–MZF/Au (Fig. 7A), the cutting of MBA-Au–DNA1/DNA2–MZF/Ag is apparently slower (Fig. 7B). It is believed that the slow process is largely due to the presence of larger assemblies (*i.e.* tetramers or pentamers) in the solution for this system. The binding of the enzyme into sites of ds-DNAs and the subsequent separation of the nanoparticles in the larger-sized assemblies are expected to be slower in terms of diffusion rate and steric hindrance than those in the smaller-sized assemblies. This assessment is supported by the difference of surface plasmon resonance bands for both MBA-Au–DNA1/DNA2–MZF/Au and MBA-Au–DNA1/DNA2–MZF/Ag assemblies (Fig. S7†). While both systems showed a clear reduction of the SP bands corresponding to MZF/Au or MZF/Ag nanoparticles in the interparticle assembly, the case of MBA-Au–DNA1/DNA2–MZF/Ag showed a small band at a longer wavelength (600–700 nm), which corresponded to somewhat larger aggregates of MZF/Ag with Au NPs (Fig. S7B†).

Note that the slower kinetic feature for the MZF/Ag case was confirmed by a control experiment performed in the absence of DNA assembly, indicating its origin from the DNA assembly process. There are several possible reasons for the difference in the enzyme cutting kinetics between the MZF/Ag and MZF/Au cases. Firstly, based on the TEM and XPS data, the MZF/Ag nanoparticles are less uniform than MZF/Au, and parts of the MZF/Ag showed indications of dumbbell structure, suggesting a non-uniform decoration of Ag components or nanoparticles around the magnetic particles was likely. This could slow down the disassembly process in comparison with the Au case. Secondly, as indicated by the enhancement factors, the surface enhancement of Ag NPs is greater than Au NPs. Thus, even when the assembly/disassembly kinetics are the same, the MZF/Ag case would show more remnant signals than the Au case, as evidenced by the fact that the decrease in the Raman intensity for enzyme cutting of MZF/Ag–DNA1/DNA2–Au is slower than the case of MZF/Au–DNA1/DNA2–Au. Finally, the propensity of surface

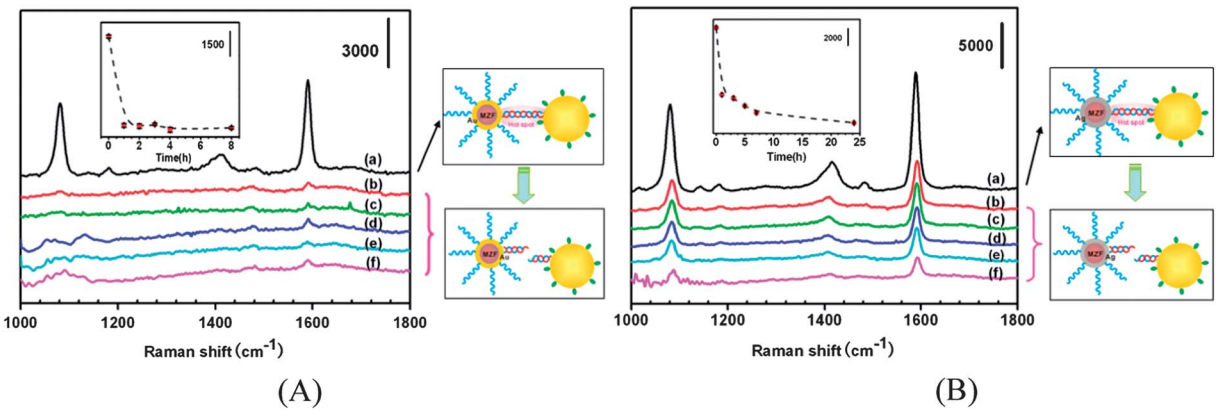

Fig. 7 SERS spectra showing (A) the change as a function of time upon introducing MspI into the solution containing MBA-Au–DNA1/DNA2–MZF/Au: (a) 0, (b) 1, (c) 2, (d) 3, (e) 4, and (f) 8 hours. (Inset: a plot of SERS intensity at 1590 cm^{-1} *vs.* enzymatic cutting time); and (B) the change as a function of time upon introducing MspI into the solution containing MBA-Au–DNA1/DNA2–MZF/Ag: (a) 0, (b) 1, (c) 3, (d) 5, (e) 7, and (f) 24 hours. (Inset: a plot of SERS intensity at 1590 cm^{-1} *vs.* enzymatic cutting time).

oxidation for Ag in comparison with the Au case could be another factor contributing the slightly lower reactivity for the Ag case.

Similar to the case of MZF/Au NPs, the MZF/Ag NPs were also demonstrated to be recyclable by the magnetic intervention after the enzyme cutting process (Fig. S8†). This process involved releasing the cut fragments of the ds-DNAs from the particle surfaces using the DTT protocol (see Scheme S1†),[46] followed by re-encapsulation of the nanoparticles by the desired capping molecules and magnetic separation. The separated nanoparticles could be re-used for the assembly process.

Conclusions

In conclusion, the gold- and silver-decorated magnetic nanoparticles have been demonstrated to be an effective bifunctional strategy for SERS detection and magnetic intervention of DNA assembly, disassembly, and enzyme cutting processes in solutions. The fact that the enhancement factors for these nanoparticle assemblies in the solution were at least one order of magnitude higher than those for unlinked nanoparticles in a solution substantiates the important role of the interparticle ds-DNA linkage for the creation of the interparticle "hot-spots". In contrast to many existing approaches that are largely based on the use of solid substrates for SERS detection, the creation of the interparticle "hot-spot" or its manipulation by the bifunctional nanoparticles in the DNA assembly, disassembly, and enzyme cutting processes provides real time biomolecular recognition, whereas the magnetic functionality allows an effective intervention of the biomolecular activity. While one of the main advantages of the bifunctional nanoprobes is the ability to detect and manipulate DNA assembly and disassembly processes in solutions and in real time, one of the potential disadvantages is the difficulty to achieve a complete coverage of the magnetic cores with Au or Ag shells, which may cause some complications in terms of reproducibility in controlling the surface reactivity due to exposures of the magnetic core surface to the solution, the latter of which could be overcome by further refining the synthesis and preparation parameters. These findings have important implications for the design of multifunctional nanomaterials for a wide range of technological applications involving biomolecular transduction and intervention, which is part of our on-going work.

Acknowledgements

This work is supported by the National Science Foundation (CHE 0848701, CMMI 1100736) and in part by the National Natural Science Foundation of China (no. 21036004). The XPS and part of TEM measurements were performed using EMSL, a national scientific user facility sponsored by the DOE and located at PNNL.

References

1 C. Kaittanis, S. Santra and J. M. Perez, *Adv. Drug Delivery Rev.*, 2010, **62**, 408.
2 N. Gilmartin and R. O'Kennedy, *Enzyme Microb. Technol.*, 2012, **50**, 87.
3 J. Theron, T. Eugene Cloete and M. de Kwaadsteniet, *Crit. Rev. Microbiol.*, 2010, **36**, 318.
4 Y. W. C. Cao, R. C. Jin and C. A. Mirkin, *Science*, 2002, **297**, 1536.
5 W. E. Doering, M. E. Piotti, M. J. Natan and R. G. Freeman, *Adv. Mater.*, 2007, **19**, 3100.
6 L. Sun and J. Irudayaraj, *J. Phys. Chem. B*, 2009, **113**, 14021.
7 L. Sun, C. Yu and J. Irudayaraj, *Anal. Chem.*, 2007, **79**, 3981.
8 S. Y. Chen and A. A. Lazarides, *J. Phys. Chem. C*, 2009, **113**, 12167.
9 D. Graham, W. E. Smith, A. M. T. Linacre, C. H. Munro, N. D. Watson and P. C. White, *Anal. Chem.*, 1997, **69**, 4703.
10 K. Faulds, W. E. Smith and D. Graham, *Anal. Chem.*, 2004, **76**, 412.
11 P. N. Njoki, I.-I. S. Lim, D. Mott, H. Y. Park, B. Khan, S. Mishra, R. Sujakumar, J. Luo and C. J. Zhong, *J. Phys. Chem. C*, 2007, **111**, 14664.
12 I.-I. S. Lim, P. N. Njoki, H. Y. Park, X. Wang, L. Wang, D. Mott and C. J. Zhong, *Nanotechnology*, 2008, **19**, 305102.

13 H. Y. Park, M. J. Schadt, L. Y. Wang, I.-I. S. Lim, P. N. Njoki, S. H. Kim, M. Y. Jang, J. Luo and C. J. Zhong, *Langmuir*, 2007, **23**, 9050.
14 I.-I. S. Lim and C. J. Zhong, *Acc. Chem. Res.*, 2009, **42**, 798.
15 K. Okamoto and D. Beach, *EMBO J.*, 1994, **13**, 4816.
16 Y. Huang, S. Zhao, M. Shi, J. Chen, Z. F. Chen and H. Liang, *Anal. Chem.*, 2011, **83**, 8913.
17 H. Yan, I.-I. S. Lim, L. C. Zhang, S. C. Gao, D. Mott, Y. Le, D. L. An and C. J. Zhong, *J. Mater. Chem.*, 2011, **21**, 1890.
18 R. A. Alvarez-Puebla and L. M. Liz-Marzán, *Chem. Soc. Rev.*, 2012, **41**, 43.
19 S. Nie and S. R. Emery, *Science*, 1997, **275**, 1102.
20 K. L. Hultman, A. J. Raffo, A. L. Grzenda, P. E. Harris, T. R. Brown and S. O'Brien, *ACS Nano*, 2008, **2**, 477.
21 H. W. Gu, K. M. Xu, C. J. Xu and B. Xu, *Chem. Commun.*, 2006, 941.
22 M. Mahmoudi, A. Simchi, M. Imani, A. S. Milani and P. Stroeve, *J. Phys. Chem. B*, 2008, **112**, 14470.
23 M. R. Jones, K. D. Osberg, R. J. Macfarlane, M. R. Langille and C. A. Mirkin, *Chem. Rev.*, 2011, **111**, 3736.
24 L. Li, T. Hutter, A. S. Finnemore, F. M. Huang, J. J. Baumberg, S. R. Elliott, U. Steiner and S. Mahajan, *Nano Lett.*, 2012, **12**, 4242.
25 X. Zhou, W. L. Xu, Y. Wang, Q. Kuang, Y. F. Shi, L. B. Zhong and Q. Q. Zhang, *J. Phys. Chem. C*, 2010, **114**, 19607.
26 B.-H. Jun, M. S. Noh, J. Y. Kim, G. S. Kim, H. M. Kang, M. S. Kim, Y. T. Seo, J. H. Baek, J. H. Kim, J. Y. Park, S. Y. Kim, Y. K. Kim, T. W. Hyeon, M. H. Cho, D. H. Jeong and Y. S. Lee, *Small*, 2010, **6**, 119.
27 C. A. Tao, Q. An, W. Zhu, H. W. Yang, W. N. Li, C. X. Lin, D. Xu and G. T. Li, *Chem. Commun.*, 2011, **47**, 9867.
28 X. M. Qian, X. Zhou and S. M. Nie, *J. Am. Chem. Soc.*, 2008, **130**, 14934.
29 Z. L. Zhang, Y. Q. Wen, Y. Ma, J. Luo, L. Jiang and Y. L. Song, *Chem. Commun.*, 2011, **47**, 7407.
30 Y. Liang, J. L. Gong, Y. Huang, Y. Zheng, J. H. Jiang, G. L. Shen and R. Q. Yu, *Talanta*, 2007, **72**, 443.
31 H. Zhang, M. H. Harpster, W. C. Wilson and P. A. Johnson, *Langmuir*, 2012, **28**, 4030.
32 H. Zhang, M. H. Harpster, H. J. Park and P. A. Johnson, *Anal. Chem.*, 2011, **83**, 254.
33 L. Y. Wang, X. Wang, J. Luo, B. N. Wanjala, C. Wang, N. Chernova, M. H. Engelhard, I.-T. Bae, Y. Liu and C. J. Zhong, *J. Am. Chem. Soc.*, 2010, **132**, 17686.
34 L. Y. Wang, J. Luo, Q. Fan, M. Suzuki, I. S. Suzuki, M. H. Engelhard, Y. Lin, N. Kim, J. Q. Wang and C. J. Zhong, *J. Phys. Chem. B*, 2005, **109**, 21593.
35 L. Y. Wang, J. Luo, M. M. Maye, Q. Fan, Q. Rendeng, M. H. Engelhard, C. Wang, Y. Lin and C. J. Zhong, *J. Mater. Chem.*, 2005, **15**, 1821.
36 E. Hao and C. G. Schatz, *J. Chem. Phys.*, 2004, **120**, 357.
37 E. Crew, H. Yan, L. Q. Lin, Z. Skeete, T. Kotlyar, N. Tchah, J. Lee, M. Bellavia, I. Goodshaw, P. Joseph, J. Luo, S. Gal and C. J. Zhong, *Analyst*, 2013, DOI: 10.1039/c3an00683b.
38 M. J. Hostetler, C. J. Zhong, B. K. H. Yen, J. Anderegg, S. M. Gross, N. D. Evans, M. D. Porter and R. W. Murray, *J. Am. Chem. Soc.*, 1998, **120**, 9396.
39 L. Y. Wang, J. Luo, S. Y. Shan, E. Crew, J. Yin, B. Wallek, S. Wong and C. J. Zhong, *Anal. Chem.*, 2011, **83**, 8688.
40 H. Yu, M. Chen, P. M. Rice, S. X. Wang, R. L. White and S. Sun, *Nano Lett.*, 2005, **5**, 379.
41 C. Wang, C. Xu, H. Zeng and S. Sun, *Adv. Mater.*, 2009, **21**, 3045.
42 X. Bao, M. Muhler, T. Schedel-Niedrig and R. Schlögl, *Phys. Rev. B: Condens. Matter Mater. Phys.*, 1996, **54**, 2249.
43 J. Salado, M. Insausti, L. Lezama, I. Gil de Muro, M. Moros, B. Pelaz, V. Grazu, J. M. de la Fuente and T. Rojo, *Nanotechnology*, 2012, **23**, 315102.
44 H. L. Liu, J. H. Wu, J. H. Min and Y. K. Kim, *J. Alloys Compd.*, 2012, **537**, 60.
45 H. M. Song, Q. S. Wei, Q. K. Ong and A. Wei, *ACS Nano*, 2010, **4**, 5163.
46 I.-I. S. Lim, U. Chandrachud, L. Y. Wang, S. Gal and C. J. Zhong, *Anal. Chem.*, 2008, **80**, 6038.
47 J. Wang, L. Wu, J. Ren and X. Qu, *Small*, 2012, **8**, 259.
48 X. Wang, X. Zhang, P. He and Y. Fang, *Biosens. Bioelectron.*, 2011, **26**, 3608.
49 K. J. Jang, H. Lee, H. L. Jin, Y. Park and J. M. Nam, *Small*, 2009, **5**, 2665.
50 D. van Lierop, K. Faulds and D. Graham, *Anal. Chem.*, 2011, **83**, 5817.
51 V. Joseph, A. Matschulat, J. Polte, S. Rolf, F. Emmerling and J. Kneipp, *J. Raman Spectrosc.*, 2011, **42**, 1736.
52 N. N. Kariuki, J. Luo, M. M. Maye, A. Hassan, T. Menard, H. R. Naslund, Y. Lin, C. Wang, M. H. Engelhard and C. J. Zhong, *Langmuir*, 2004, **20**, 11240.
53 D. I. Gittins and F. Caruso, *ChemPhysChem*, 2002, **3**, 110.

